Journal of Catalysis **194,** 198–210 (2000)
doi:10.1006/jcat.2000.2941, available online at http://www.idealibrary.com on IDEAL®

CO_2/CH_4 Reforming over Ni–La_2O_3/5A: An Investigation on Carbon Deposition and Reaction Steps

J. Z. Luo, Z. L. Yu,[1] C. F. Ng, and C. T. Au[2]

Department of Chemistry, Hong Kong Baptist University, Kowloon Tong, Kowloon, Hong Kong, China

Received November 8, 1999; revised May 31, 2000; accepted May 31, 2000

Carbon deposition and reaction pathways in CO_2/CH_4 reforming over Ni–La_2O_3/5A have been studied by means of XRD, *in situ* **TG, pulse experiments, chemical trapping, TEM, and EPR. The XRD results revealed that due to the formation of perovskite-like La_2NiO_4 phase in Ni–La_2O_3/5A, the small-size (ca. 9 nm) Ni^0 crystallites formed in H_2 reduction remained unsintered during 48 h of on-stream reaction at 800°C. The accumulation of carbon on the active sites was the main reason for Ni–La_2O_3/5A deactivation. The detection of $^{13}CO_2$ and CO_2 in O_2 pulsing onto a sample pretreated with $^{13}CH_4/CO_2$ confirmed that the deposited carbon was from both CH_4 and CO_2. The $^{13}CO_2/CO_2$ molar ratio decreased with the rise in temperature, indicating that the contribution of CO_2 toward deposited carbon was larger than that of CH_4 at higher temperatures. In CO and CO_2/CH_4 atmospheres, we observed similar TG patterns and obtained identical TEM images of deposited carbon; we propose that carbon deposition is mainly via CO disproportionation. The observation of CD_3COOH in CD_3I chemical trapping experiments suggested that HCOO was an intermediate of CO_2/CH_4 reforming. The amount of CO_2 converted was roughly proportional to the amount of H present on the catalyst surface. These results indicate that CO_2 activation could be H-assisted. Pulsing CH_4 onto a H_2-reduced Ni–La_2O_3/5A catalyst and a similar catalyst treated with CO_2, we found that CH_4 conversion was higher in the latter case. Hence, the idea of oxygen-assisted CH_4 dissociation is plausible. As for methane conversion, k_H/k_D of 1.2 and 1.1 at 600 and 700°C, respectively, were observed, implying that C–H cleavages are slow kinetic steps in CH_4/CO_2 reforming. Based on these experimental results, we have derived reaction pathways for CO_2/CH_4 reforming, the decomposition of CH_xO ($x = 1$ or 2) is considered to be the rate-determining step for syngas formation.**

Key Words: **CO_2/CH_4 reforming; Ni–La_2O_3/5A; nickel catalyst; carbon deposition; reaction mechanism; chemical trapping; isotope effect.**

INTRODUCTION

The CO_2 reforming of methane for the production of syngas with H_2/CO ratios suitable for F-T synthesis has aroused renew interest in recent years. In addition to various applications in chemical energy transmission (1–4), the conversion of CH_4 and CO_2 to value-added chemicals makes the CO_2/CH_4 reforming process attractive. Catalysts such as transition metal carbides and sulfides, unsupported metals, and supported Group VIII metals have been investigated extensively for the reaction (5). It has been reported that catalyst deactivation due to carbon deposition is a serious problem (6, 7). A number of calculations on the thermodynamic potential of graphitic carbon deposition as related to reaction conditions suggested that carbon formation could be avoided thermodynamically at high temperatures (e.g., 1000°C) and with CO_2/CH_4 ratios bigger than unity (8–10). However, from a standpoint of industry, it is desirable to operate the process at a relatively lower temperature and with a CO_2/CH_4 ratio close to unity. This necessitates the use of a catalyst which could inhibit carbon formation under thermodynamically favorable conditions. Noble metals such as Rh and Ru are known to reduce carbon deposition (11, 12). However, considering the high cost and limited availability of these precious metals, it is more attractive to develop a suitable nickel catalyst to tackle the problem of carbon deposition. The origin of deposited carbon may be via CH_4 decomposition

$$CH_4 \rightarrow C + 2H_2 \quad \Delta H^\circ = 75.2\,\text{kJ mol}^{-1}$$

or CO disproportionation

$$2CO \rightarrow C + CO_2 \quad \Delta H^\circ = -173.0\,\text{kJ mol}^{-1}.$$

In general, carbon deposition can be reduced if nickel is supported on a metal oxide of strong basicity (13–15). It has been suggested that the increase in basicity of the support materials would promote CO_2 chemisorption. The increase in the concentration of adsorbed CO_2 hinders the formation of deposited carbon via reverse CO disproportionation. On the other hand, carbon deposition is closely related to

[1] On leave from Chengdu Institute of Organic Chemistry, Chinese Academy of Sciences.

[2] To whom correspondence should be addressed. E-mail: pctau@hkbu.edu.hk.

0021-9517/00 $35.00

catalyst structures. For example, Ni_2AlO_4 spinel formed during preparation could markedly reduce carbon deposition over Ni/Al_2O_3 in CO_2/CH_4 reforming (16). The great difference in apparent activation energies for the reduction of NiO (18.0 kJ mol^{-1}) and $NiAl_2O_4$ (133.8 kJ mol^{-1}) is indicative of a stronger Ni–O bond in the latter compound (17). It has been reported that the reduction of $NiAl_2O_4$ would result in the formation of small-surface Ni crystallites which are resistant to sintering and carbon formation (18). Several recent publications have demonstrated that NiO–MgO solid solutions could stabilize small Ni particles and prolong catalyst lifetime (19–21). Zhang *et al.* (22, 23) attributed the improvement in catalytic activity and the reduction in carbon formation observed over a reduced Ni/La_2O_3 catalyst to the isolation of nickel ensembles by LaO_x.

To develop a high performance catalyst, it is necessary to clarify the reaction mechanism and to identify the rate-determining steps. After investigating the isotopic kinetic effects over Ni/SiO_2 (24) and Rh/SiO_2 (25), Wang and Au concluded that CH_4 dissociation was a rate-determining step. Similar conclusions were drawn by Kim *et al.* (26) and Zhang *et al.* (27). Nakamura *et al.* (28) suggested that the step for CO_2 dissociation was rate-determining over supported Rh catalysts. However, Solymosi and co-workers (29, 30) considered that the activation and dissociation of CO_2 did not play an important role in the reforming of methane over a supported Rh catalyst. In addition, the idea of oxygen-assisted CH_4 dissociation has been suggested before. Nevertheless, Bradford and Vannice suggested that adsorbed O was unlikely to promote CH_4 dissociation (5, 21, 31). Based on the results of pulse surface reaction analysis (PSRA), Osaki *et al.* (32, 33) proposed that surface reaction of CH_x and O was a rate-determining step. Bradford and Vannice established a kinetic model in which CH_xO decomposition was thought to be a slow step (5, 21, 31). With these discrepancies in understanding, it is necessary to look further into the mechanism of the reaction.

In the present work, CO_2/CH_4 reforming over Ni–La_2O_3/5A catalysts has been studied by XRD, *in situ* TG, pulse experiments, chemical trapping, TEM, and EPR. We selected 5A molecular sieve for its good affinity to CO_2. We found that by using La_2NiO_4 as a precursor, the Ni^0 particles formed in hydrogen reduction were separated and stabilized; as a result, catalyst lifetime was prolonged. A mutual effect on the activation of CH_4 and CO_2 has been proposed.

EXPERIMENTAL

1. Catalyst Preparation

The Ni–La_2O_3/5A catalyst was prepared by adopting the citric acid complexing method. We added 6.3 g of 5A molecule sieve to a mixed solution of $Ni(NO_3)_3 \cdot 6H_2O$ (0.5 M, 18.8 ml), $La(NO_3)_3 \cdot 6H_2O$ (0.5 M, 37.6 ml), and citric acid (6 g). The resultant gel was heated and stirred continually until a viscous syrup was formed. The residue was calcined in air at 500°C for 4 h and then at 850°C for 6 h. The NiO loading of the catalyst was 10 wt%. Before testing, the catalyst (50 mg) was first reduced *in situ* at 500°C in a flow of H_2 (20 ml min^{-1}) for 1 h.

2. Catalyst Test

The catalysts were tested in a fixed-bed continuous flow quartz microreactor (i.d. = 4 mm) at atmospheric pressure. The flow rate of the reactant mixture (CO_2/CH_4 molar ratio = 1) was 40 ml min^{-1}. The effluent was analyzed on line by a TCD gas chromatography (Shimadzu −8A) with Spherocarb and Porapak Q columns.

3. In Situ TG

The deposition and reactivity of carbon on the catalyst were examined using a thermal gravimeter (TG) (Shimadzu DT-40). The molar composition of reactant mixture was $CH_4/N_2 = 1/3$ for methane decomposition, $CO/N_2 = 1/3$ for CO disproportionation, and $CO_2/CH_4/N_2 = 1/1/2$ for CO_2/CH_4 reforming. The total flow rate was 40 ml min^{-1}. The sample (10 mg) was first reduced in H_2 at 500°C for 1 h in a fixed-bed continuous flow microreactor and then cooled down to 25°C and transferred to the quartz sample holder (i.d. = 3 mm) in air. After purging with reactant mixture at room temperature for 10 min, the sample was program-heated to 800°C at a rate of 20°C min^{-1}. The weight change of the sample was simultaneously recorded. After carbon deposition, a flow of CO_2/N_2 (1/1, 40 ml min^{-1}) mixture was introduced to the catalyst and the weight loss was monitored at 800°C. As for the investigation of carbon deposition at working conditions, after heating the reduced sample to the reaction temperature in N_2, we introduced the reactant mixture to the catalyst and monitored the weight increase at the same temperature.

4. Pulse Experiment

In the pulse experiment, the catalyst (20 mg) was placed in a quartz microreactor and reduced in a H_2 flow (10 ml min^{-1}) at 500°C for 1 h, followed by heating to the reaction temperature in a flow of He (10 ml min^{-1}). In each pulsing, 67.5 μl of CH_4, CO_2, CO, O_2, $^{13}CH_4/CO_2$, CH_4/CD_4, CH_4/CO_2 or CD_4/CO_2 (molar ratio, 1/1) was injected into the system. The effluent gases were monitored on line by a mass spectrometer (HP G-1800A). In order to identify the products correctly, we have taken into account the interference due to isotopes and fragments.

5. Chemical Trapping

In the chemical trapping experiments, the catalyst (20 mg) was placed in a quartz microreactor and reduced

in a H_2 flow (10 ml min^{-1}) at 500°C for 1 h, followed by heating to the reaction temperature in a flow of He (10 ml min^{-1}). We first pulsed CO_2/CH_4 (molar ratio, 1/1) onto the sample until a steady state was reached, then CD_3I (5 μl) and reactant mixture were injected into the system. The carrier gas was He (10 ml min^{-1}) and the pulse size was 67.5 μl. The outlet gases were analyzed on line by a mass spectrometer (HP G-1800A). The interference due to isotopes and fragments was taken into account in order to identify the products correctly.

6. Catalyst Characterization

Chemisorption experiments were conducted in a quartz microreactor at room temperature. The sample was first reduced in H_2 at 500°C for 1 h, followed by cooling in H_2 to room temperature and He purging for 10 min. We kept on pulsing CO to the catalyst until there was no observable increase in CO signal intensity. The uptake of CO was then estimated and used to calculate Ni metal dispersion and particle size, assuming that each surface Ni site chemsorbs one CO molecule, i.e., $CO/Ni_{surface} = 1$.

The specific surface areas of the catalysts were measured by the BET method using a NOVA-1200 instrument. The phase compositions were determined by a X-ray diffractrometer (XRD, Rigaku D-MAX) with monochoromatized Cu$K\alpha$ radiation ($\lambda = 0.15406$ nm). The Ni particle size was estimated according to the half height width of the Ni (111) peak obtained in XRD investigation.

TEM images of deposited carbon were taken by means of a JEM-100CX (JEOL) operated at 100 KV. The sample of deposited carbon was treated with 3 M HNO_3 and then dispersed by supersonic waves in aqueous surfactant solution before mounting on a Cu grid for TEM observation.

The electron paramagnetic resonance (EPR) experiments were carried out on a JES-TS100 spectrometer. Samples (ca. 1.5 g) treated under various conditions were examined in the X-band at 25°C. The EPR system was equipped with a quartz-tube reactor which was transferable conveniently between the sample chamber and an oven. The sample in the quartz reactor could be heated to 800°C and exposed to gas(es) without being exposed to air.

RESULTS

1. The Physicochemical Properties of Ni–La_2O_3/5A Catalysts

Table 1 shows the physicochemical properties of Ni–La_2O_3/5A. According to the patterns (not shown) obtained in XRD investigations, strong signals of La_2NiO_4 and 5A phases as well as weak signals of Al_2O_3 and SiO_2 phases were observed. After reduction in H_2 at 500°C, nickel existed mainly as Ni^0 particles, with the diameter estimated to be ca. 9 nm. After 48 h of on-stream CO_2/CH_4 reforming, there were no significant changes in phase composition and Ni^0 particle size. The results indicated that the Ni–La_2O_3/5A catalyst was stable during the reforming reaction. Based on the amount of chemisorbed CO (46 μmol g^{-1}), Ni dispersion was estimated to be ca. 3.4%. The specific surface area of 5A molecular sieve was ca. 300 $m^2\ g^{-1}$; for the Ni–La_2O_3/5A catalyst, it was 157 $m^2\ g^{-1}$. Such a drastic drop in surface area might be caused by the formation of new phases and/or the collapse of 5A crystallite during the preparation process. It should be noted that the diameter of nickel particles estimated by CO chemsorption was 29 nm, about 3 times that (9 nm) estimated according to XRD line broadening.

TABLE 1

Physicochemical Properties of the Ni–La_2O_3/5A Catalyst

Specific surface area (m^2/g)	CO uptake (μmol/g)	Ni dispersion[a] (%)	Ni particle size[a] (nm)	Ni particle size[b] (nm)
157	46	3.4	29	9

[a] Based on CO chemisorption data.
[b] Based on XRD results.

2. Catalytic Performance

The catalytic performance of Ni–La_2O_3/5A is shown in Table 2. At 450°C, a significant amount of syngas was formed. With the rise in temperature, the conversions of CO_2 and CH_4 increased. At 800°C, CO_2 and CH_4 conversions were 79.7 and 92.1%, respectively. Stoichiometrically, CO_2 and CH_4 conversions should be the same at CO_2/CH_4 molar ratio $= 1$ if syngas is the only product. From Table 2, however, one observes that CH_4 conversion was lower than CO_2 conversion at or below 650°C; whereas above 650°C, it was the other way around. The unequivalence of CO_2 and CH_4 conversions reveals the presence of secondary

TABLE 2

The Performance of Ni–La_2O_3/5A for the Production of Syngas in CO_2/CH_4 Reforming

Temp. (°C)	Conv. (%)		TOF (s^{-1})			
	CH_4	CO_2	CH_4	CO_2	CO	H_2
450	3.23	4.37	0.21	0.28	0.49	0.25
500	8.25	9.52	0.53	0.62	1.15	0.58
550	16.34	17.12	1.06	1.11	2.17	1.53
600	29.02	30.31	1.88	1.96	3.84	3.02
650	42.61	44.33	2.76	2.87	5.63	4.83
700	63.25	59.02	4.09	3.82	7.91	7.15
750	80.71	72.86	5.22	4.71	9.94	9.24
800	92.12	79.74	5.96	5.16	11.12	10.44

Note. Reaction conditions: feedstock CH_4/CO_2 molar ratio = 1; GHSV = 48,000 ml $h^{-1}\ g^{-1}$.

reactions under the reaction conditions adopted. The detection of H_2O in the outlet was a clear indication of the occurrence of the reverse water gas shift (RWGS) reaction.

The stability of the Ni–La_2O_3/5A catalyst at 800°C was investigated. The conversions of CO_2 and CH_4 decreased only moderately with time. Over a period of 48 h, CO_2 and CH_4 conversions decreased gradually from the initial values of 79.7 and 92.1%, respectively, to 75.0 and 80.2%.

3. *TG and TEM Studies*

Figure 1 shows the TG profiles of Ni–La_2O_3/5A in a flow of CH_4/N_2, CO/N_2, and $CO_2/CH_4/N_2$. In a CH_4/N_2 flow (Fig. 1a), weight gain started at 585°C and increased rapidly to reach a plateau at 635°C. In a CO/N_2 flow (Fig. 1b), the threshold temperature for weight gain was at 460°C, and between 460 and 580°C there was a linear rise in weight gain with a plateau appearing above 580°C. The amounts of weight gain in CH_4 decomposition and CO disproportionation were 100 and 80 mg g^{-1}, respectively. In a $CO_2/CH_4/N_2$ flow, the onset temperature for weight gain was 650°C (Fig. 1c), a plateau was reached after a period of ca. 10 min at 800°C; the weight gain was 60 mg g^{-1}. If we introduced a flow of CO_2/N_2 at 800°C to the catalyst over which a plateau had been observed, significant weight loss took place; at or below 700°C, such a weight loss was not obvious. It is clear that at 800°C, the accumulated carbonaceous species became reactive towards CO_2.

Figure 2 shows the TEM images of deposited carbon collected after the Ni–La_2O_3/5A catalyst had been heated from room temperature to 800°C and then kept at 800°C for 10 min in various atmospheres, respectively. It is apparent that there were encapsulated as well as whisker carbon. The former was mostly formed in a CH_4/N_2 atmosphere,

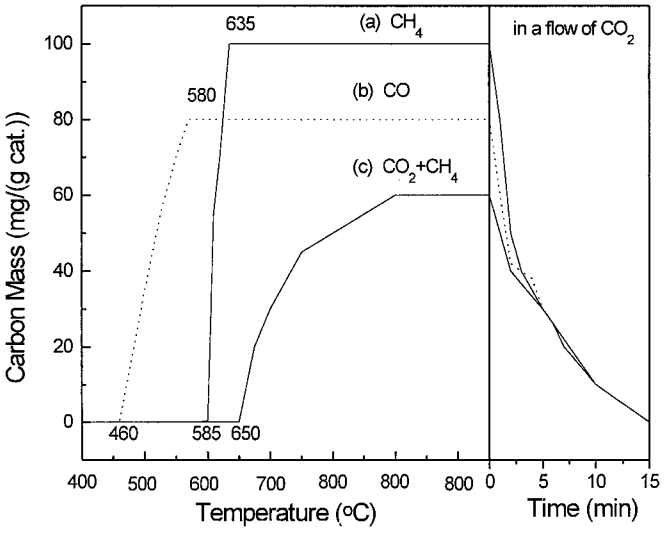

FIG. 1. *In situ* TG profiles of Ni–La_2O_3/5A kept in (a) CH_4, (b) CO, and (c) CH_4/CO_2 (1/1) before exposure to a flow of CO_2 at 800°C.

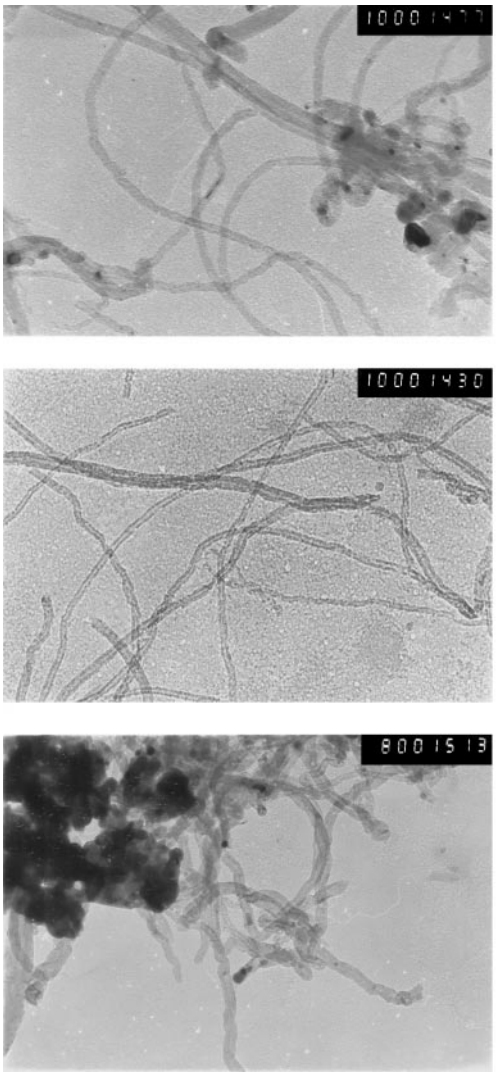

FIG. 2. TEM images of deposited carbon formed in (a) CO_2/CH_4; (b) CO; (c) CH_4 atmosphere.

whereas the latter was formed in a CO/N_2 or $CO_2/CH_4/N_2$ atmosphere. The whisker carbon formed in CO/N_2 atmosphere was estimated to be 5 ~ 15 nm in diameter. When the catalyst was exposed to a $CO_2/CH_4/N_2$ atmosphere, the diameter of the whisker carbon was in the range of 5 ~ 25 nm.

Figure 3 shows the amounts of carbon deposited on Ni–La_2O_3/5A as related to reaction time at various temperatures in CH_4/N_2, CO/N_2, and $CO_2/CH_4/N_2$ atmospheres, respectively. In a CH_4/N_2 atmosphere, the amount of deposited carbon augmented gradually with time and reached a constant value after ca. 40 min; the amount of carbon deposited increased with reaction temperature. In a CO/N_2 atmosphere, carbon deposition reached a constant value within 20 min and the extent of carbon deposition decreased with temperature rise. As for a $CO_2/CH_4/N_2$

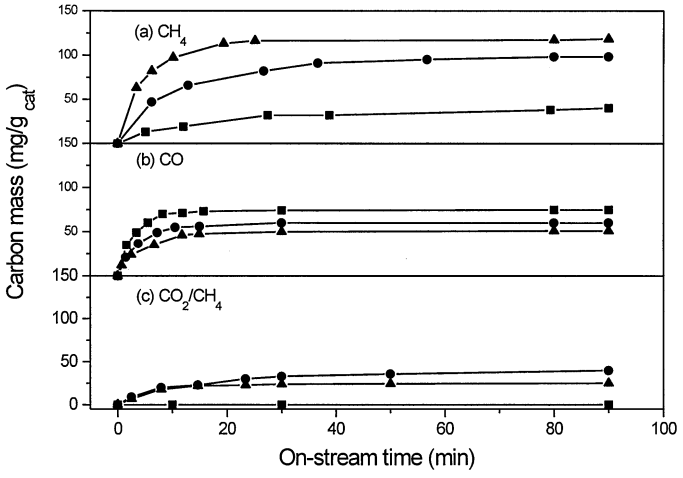

FIG. 3. TG profiles of Ni–La_2O_3/5A versus time on stream at 600 (■), 700 (●), and 800°C (▲) in various atmospheres: (a) CH_4, (b) CO, and (c) CO_2/CH_4.

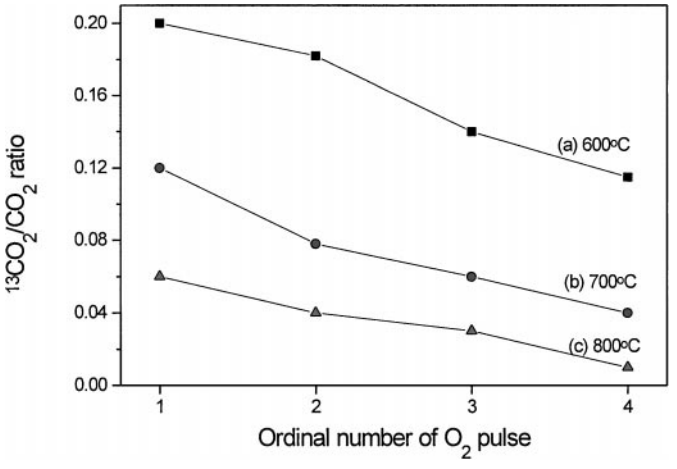

FIG. 5. $^{13}CO_2/CO_2$ ratio versus O_2 pulse number after 5 pulses of $^{13}CH_4/CO_2$ at (a) 600, (b) 700, and (c) 800°C over Ni–La_2O_3/5A.

atmosphere, there was no carbon deposition at 600°C. At 700 or 800°C, the deposition of carbon increased rather gradually with time; the amount of carbon deposited at 700°C was larger than that deposited at 800°C.

4. *$^{13}CH_4/CO_2$ Pulse Experiment*

In order to investigate the origin of deposited carbon and the reaction mechanism of CO_2/CH_4 reforming, $^{13}CH_4/CO_2$ pulse experiments were performed. We pulsed $^{13}CH_4/CO_2$ (molar ratio, 1/1) at a desired temperature onto the Ni–La_2O_3/5A catalyst which had been H_2-reduced at 500°C for 1 h and monitored the $^{13}CO_2/CO_2$ ratio (Fig. 4). After 5 pulses of $^{13}CH_4/CO_2$, the deposited carbon was treated with 4 O_2 pulses at the same temperature; the $^{13}CO_2/CO_2$ ratio (Fig. 5) and the amount of $^{13}CO_2$ generated (Fig. 6) were monitored. The signal with $m/z = 45$ detected in the pulse experiments was attributed to $^{13}CO_2$ because its intensity was much stronger than the expected contribution (1%) of natural isotopic carbon in CO_2; also, we detected no formation of formic acid (main peaks at $m/z = 45$ and 46). Over the H_2-reduced Ni–La_2O_3/5A sample, with the increase of $^{13}CH_4/CO_2$ pulse number, the $^{13}CO_2/CO_2$ ratio increased; such an increase was the most obvious at 600°C (Fig. 4). It indicated that the accumulation and oxidation of ^{13}C species (derived from $^{13}CH_4$ dissociation) had taken place on the catalyst. The CH_4 and CO_2 conversions at

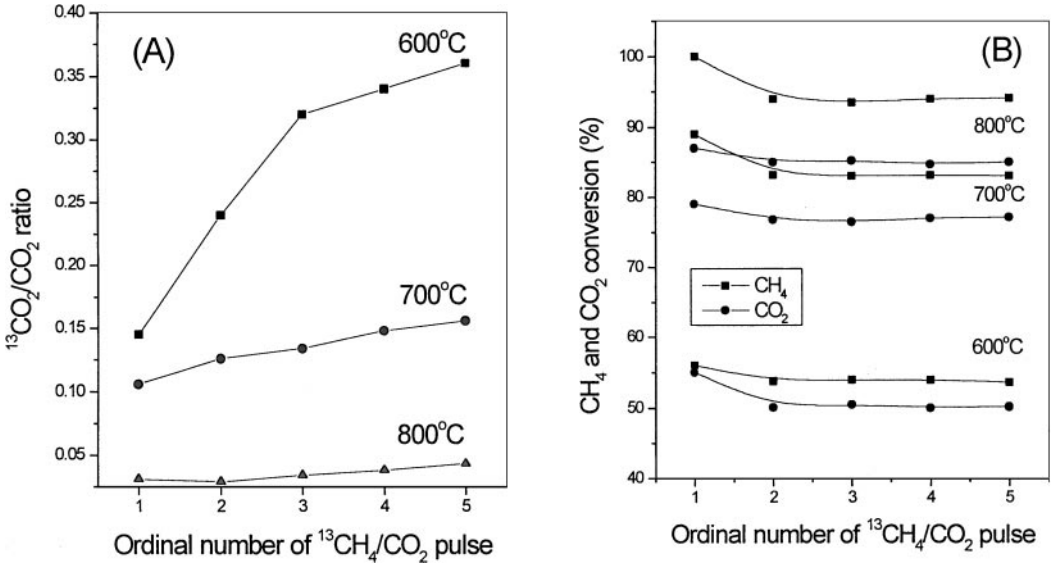

FIG. 4. (A) $^{13}CO_2/CO_2$ molar ratio and (B) CH_4 and CO_2 conversions versus CH_4/CO_2 pulse number at various tempertures over prereduced Ni–La_2O_3/5A.

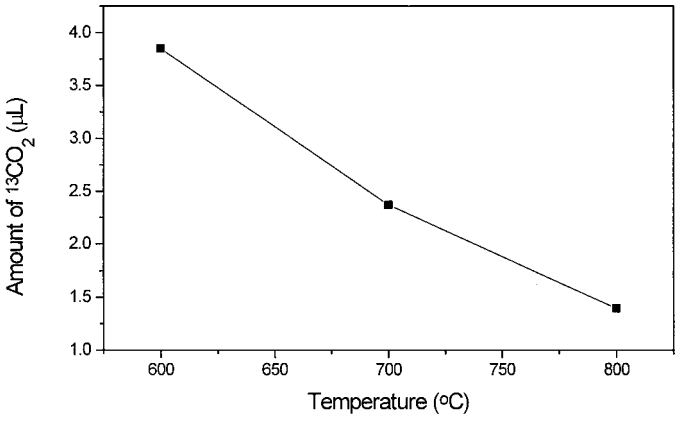

FIG. 6. The total amount of $^{13}CO_2$ generated in 4 pulses of O_2 versus temperature over a Ni–La_2O_3/5A sample treated with 5 pulses of $^{13}CH_4/CO_2$.

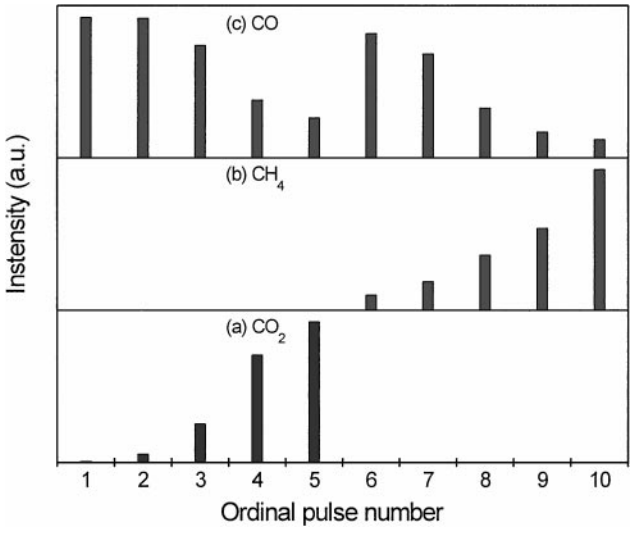

FIG. 7. The MS signals of (a) CO_2, (b) CH_4, and (c) CO detected in five pulses of CO_2 followed by 5 pulses of CH_4 over H_2-reduced Ni–La_2O_3/5A at 800°C.

various tempertures are also shown in Fig. 4. One can observe that after the first pulse of $^{13}CH_4/CO_2$, the CH_4 and CO_2 conversions stayed almost unchanged with the rise in the pulse number. The somewhat higher conversions in the first pulse might be due to the initial adsorption of CH_4 and CO_2 on the catalyst. When O_2 was then pulsed onto the sample, there was no O_2 ($m/z = 32$) detected in the effluent; the O_2 must have been consumed in the oxidation of surface species and/or adsorbed by the reduced catalyst. As both $^{13}CO_2$ and CO_2 were detected in the effluent, one can affirm that in CO_2/CH_4 reforming, both CH_4 and CO_2 contributed to the formation of deposited carbon. The $^{13}CO_2/CO_2$ molar ratio decreased with O_2 pulse number (Fig. 5), suggesting that the ^{13}C species originated from $^{13}CH_4$ was more reactive toward O_2 than the ^{12}C species from CO_2. The total amount of $^{13}CO_2$ produced in 4 pulses of O_2 (Fig. 6) and the $^{13}CO_2/CO_2$ molar ratio obtained over Ni–La_2O_3/5A pretreated with 5 pulses of $^{13}CH_4/CO_2$ (Fig. 5) decreased with the rise in temperature. That is to say, depending upon reaction temperature, the contribution of CH_4 and CO_2 in CO_2/CH_4 reforming toward carbon deposition varied.

5. *Pulse Experiments*

5.1. CO_2–CH_4. Figure 7 shows the results of introducing 5 pulses of CO_2 followed by 5 pulses of CH_4 to a H_2-reduced Ni–La_2O_3/5A sample at 800°C. The generation of CO in CO_2-pulsing was an indication of CO_2 dissociation and partial oxidation of the reduced catalyst. We observed that CO_2 conversion and CO yield decreased with CO_2 pulse number. When CH_4 was pulsed in after the 5 pulses of CO_2, we detected CO in the outlet. These results illustrated that the surface O species generated in CO_2 dissociation reacted with CH_4 to produce CO. Like results were obtained at 600 and 700°C. The amounts of CO_2 and CH_4 converted and the amount of CO produced are listed in Table 3. The amounts of consumed CO_2 and CH_4 increased remarkably with the rise in temperature. In the CO_2 pulses, the amount of CO_2 consumed was more than that of CO produced and the difference, Δ, increased with a rise in temperature.

5.2. CH_4–CO_2. Figure 8 shows the profiles of 5 pulses of CH_4 followed by 5 pulses of CO_2 over a H_2-reduced Ni–La_2O_3/5A sample at 800°C. The increase in CH_4 intensity with the advance in CH_4 pulse number indicated that CH_4 decomposition was more substantial in the first few pulses. After the five pulses of CH_4, with the pulsing of CO_2 onto the catalyst, we detected CO. Similar results were observed at 600 and 700°C. The amounts of CH_4 and CO_2 consumed and CO produced are listed in Table 4. The amount of converted CH_4 increased with the rise in temperature. At or above 700°C, CO_2 dissociated to CO and O. The C species generated in CH_4 decomposition reacted with the O originated from CO_2 to produce CO, causing the amount of CO produced to exceed the amount of CO_2 converted as reflected by the negative values of Δ.

TABLE 3

The Total Amounts of Converted CO_2 and CH_4 and the Total Amount of CO Generated in the Pulsing of CO_2 and CH_4 over H_2-Reduced Ni–La_2O_3/5A as Illustrated in Fig. 7

Temp. (°C)	CO_2 pulse			CH_4 pulse		CH_4/CO_2 pulse[a]
	CO_2 (μl)	CO (μl)	Δ (μl)	CH_4 (μl)	CO (μl)	CO (μl)
600	8.1	6.0	2.1	8.8	1.4	280
700	58.7	55.3	3.4	114.3	36.5	480
800	293.0	283.5	9.5	308.5	219.4	614

Note. Δ is the difference between the amount of CO_2 converted and the amount of CO produced.

[a] Produced from 10 pulses of CO_2/CH_4 (1 : 1 in molar).

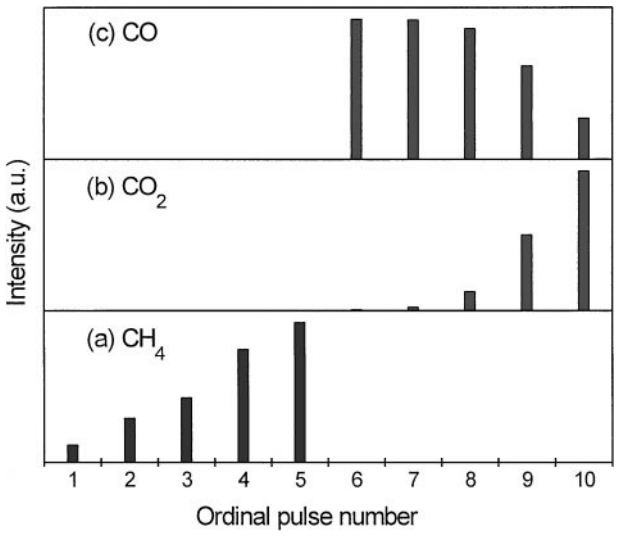

FIG. 8. The MS signals of (a) CH_4, (b) CO_2, and (c) CO detected in five pulses of CH_4 followed by 5 pulses of CO_2 over H_2-reduced Ni–La_2O_3/5A at 800°C.

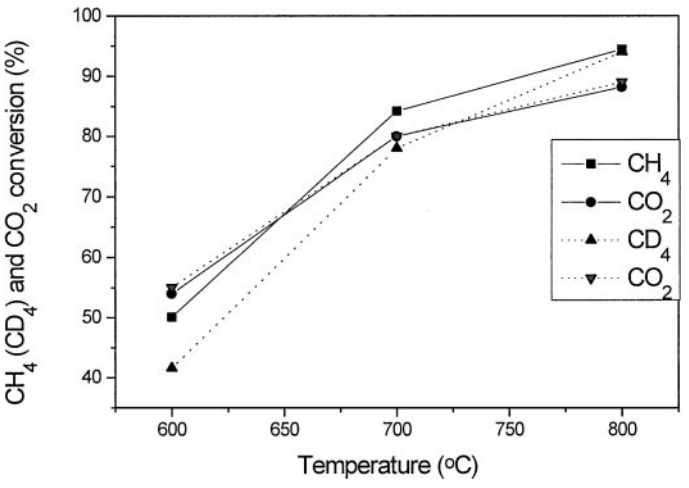

FIG. 9. The conversion of methane and CO_2 versus temperature over H_2-reduced Ni–La_2O_3/5A in CH_4/CO_2 and CD_4/CO_2 (dotted lines) pulse experiments.

5.3. CH_4/CO_2 and CD_4/CO_2. CH_4/CO_2 pulsing over H_2-reduced Ni–La_2O_3/5A was investigated at 600, 700, and 800°C, respectively (Fig. 9). Both CH_4 and CO_2 conversions increased with the rise in reaction temperature. At 600°C, CH_4 conversion (50%) was lower than CO_2 conversion (54%), while at 700 and 800°C, CH_4 conversions (83 and 93%) were higher than the CO_2 conversions (77 and 85%), respectively. These results are consistent with the data obtained in the continuous flow reactor (Table 1). The total amounts of CO produced in 10 pulses of CH_4/CO_2 are also listed in Table 3. One can observe that the total amount of CO produced in 10 pulses of CH_4/CO_2 was much larger than that obtained in 5 pulses of CO_2 and then 5 pulses of CH_4.

The results of CD_4/CO_2 pulsing are also illustrated in Fig. 9. Compared to the results of CH_4/CO_2 pulsing, deuterium isotope effect on methane conversion was observed at 600 and 700°C, but not at 800°C. There was no obvious isotope effect on the conversion of CO_2. The ratios of CH_4 and CD_4 conversions were 1.2 and 1.1 at 600 and 700°C, respectively.

TABLE 4

The Total Amounts of Converted CH_4 and CO_2 and the Total Amount of CO Generated in the Pulsing of CH_4 and CO_2 over H_2-Reduced Ni–La_2O_3/5A as Illustrated in Fig. 8

Temperature (°C)	CH_4 pulse		CO_2 pulse		
	CH_4 (μl)	CO (μl)	CO_2 (μl)	CO (μl)	Δ (μl)
600	1.3	0.0	13.0	14.0	−1.0
700	67.5	0.0	101.2	114.8	−13.6
800	113.4	4.2	303.8	336.8	−33.0

Note. Δ is the difference between the amount of CO_2 converted and the amount of CO produced.

5.4. CH_4/CD_4. Figure 10 illustrates the methane conversion and methane isotopic distribution after a pulse of CH_4/CD_4 (molar ratio, 1/1) over Ni–La_2O_3/5A. At 600°C, the CH_4 and CD_4 conversions were 4.0 and 3.7%, respectively, resulting in R_H/R_D of 1.08. At 700°C, the corresponding conversions were 12.9 and 12.5%, resulting in $R_H/R_D = 1.03$. Theoretically, if the breaking of the C–H bond was the rate-determining step for methane activation, the R_H/R_D should be 1.99 and 1.86 at reaction temperatures of 600 and 700°C, respectively (34). The near unity of R_H/R_D in CH_4/CD_4 pulsing indicated that the dehydrogenation of methane over Ni–La_2O_3/5A was largely reversible, i.e., $CH_4 \Leftrightarrow CH_x + (4-x)H$.

6. Chemical Trapping

Adding an alkylation reagent to convert surface formyl species into the corresponding aldehyde or carboxylic acid is a common method of chemical trapping. Methyl iodide, a highly effective trapping reagent, has been widely used (35). Following the introduction of 5 μl of CD_3I onto a catalyst at working conditions, CD_3COOH ($m/z = 63$), CD_3OCD_3 ($m/z = 52$), CD_3CHO ($m/z = 47$), as well as CD_4 ($m/z = 20$), DCO_2D ($m/z = 48$), and D_2CO ($m/z = 32$) were detected. No ethane or ethene was observed. Figure 11 shows the relative intensities of the products. When COOH, O, and CHO were trapped by CD_3 radicals, CD_3COOH, CD_3OCD_3, and CD_3CHO were the expected products. The generation of CD_4, DCO_2D, and D_2CO were less expected. It is apparent that the CD_3 radical generated in CD_3I dissociation could further decompose to give D which reacted with surface CD_3, CO_2, and CO to produce, respectively, CD_4, DCO_2D, and D_2CO. Although with lower intensities,

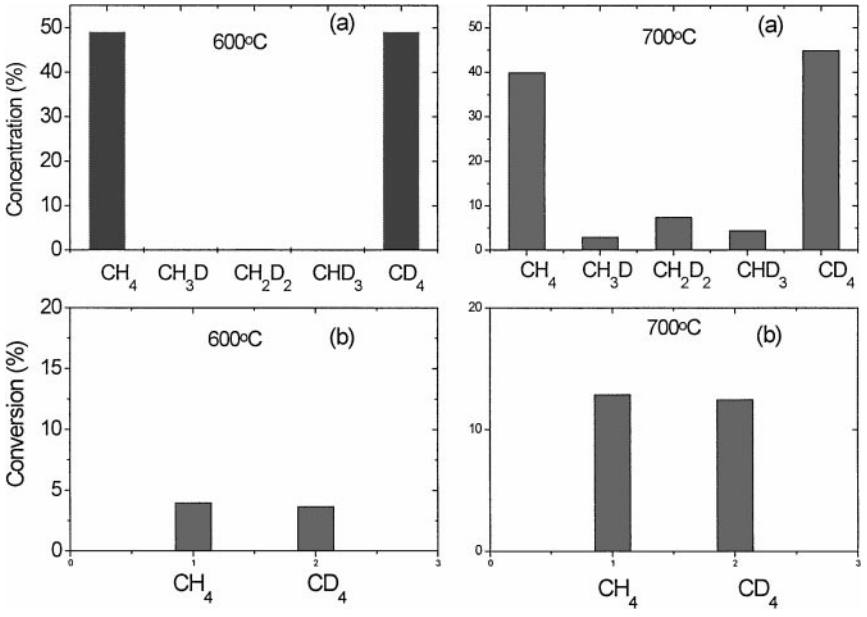

FIG. 10. (a) Distribution of isotopic methane species and (b) conversion of methane after a single pulse of CH_4/CD_4 (1/1) reaction over Ni–La_2O_3/5A at 600 and 700°C.

signals due to isotopic H/D exchanged formic acid ($m/z = 46$) and formaldehyde ($m/z = 30$) were detected. The presence of CD_3COOH, CD_3CHO, and CD_3OCD_3 implied that there were COOH, CHO, and O on the catalyst.

7. *EPR Studies*

Figure 12 shows the EPR profiles of the catalyst after H_2-reduction at 400°C. A strong and smooth line centered at around $g = 2.4$ was observed over a Ni–La_2O_3/5A sample that had been H_2-reduced at 500°C for 1 h. The strong signal could be attributed to metallic nickel (36). In order to minimize the disturbance due to metallic nickel, we employed a 0.5 wt% Ni–La_2O_3/5A sample for EPR investigation. For comparison purposes, a La_2O_3–5A sample was also investigated. No EPR signal was observed over the fresh 0.5 wt% Ni–La_2O_3/5A catalyst. After reduction at 400°C for 0.5 h, a narrow symmetric peak centered at $g = 2.003$ with a width of 10 G appeared. This signal could be assigned to trapped electrons (36). Exposure of the catalyst to air at room temperature caused this signal to decrease in intensity by ca. 30%, possibly due to the coupling interaction between paramagnetic gaseous O_2 and the trapped electrons on the surface. This result implied that ca. 30% of the trapped electrons were on the surface. The peak heights of the trapped electron signals detected over 0.5 wt% Ni–La_2O_3/5A as well as that detected over La_2O_3–5A versus reduction temperature are shown in Fig. 13. With the rise in reduction temperature to 400°C, the signal intensity of trapped electrons increased to a maximum value. Further treatment above 400°C would cause the signal to decrease, a result of interaction among the increased population of trapped electrons. It is clear that the intensity of trapped electrons detected over 0.5 wt% Ni–La_2O_3/5A was much higher than that over La_2O_3/5A.

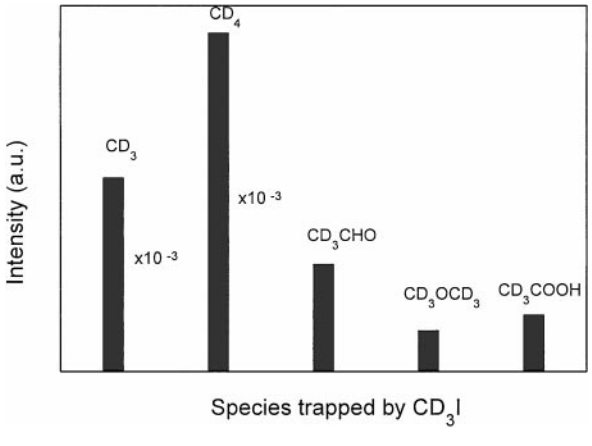

FIG. 11. Patterns of CHO, O, and COOH trapped by CD_3I over Ni–La_2O_3/5A. For comparison, the patterns of CD_3 and CD_4 are also shown.

DISCUSSION

1. *Catalytic Performance*

In Table 1, one can observe that the diameter of nickel particles deduced from CO chemisorption was 29 nm, which is about 3 times that (9 nm) estimated according to the Scherrer equation. Over a 17 wt% Ni/La_2O_3 catalyst, Verykios *et al.* (23, 37) observed that the nickel particle size (110 ~ 324 nm) deduced from H_2 and CO chemisorption

was up to 3 ~ 10 times that (33 nm) estimated according to the XRD line broadening results. They attributed this to the decoration of the nickel particle by LaO_x originating from the support. According to the XRD results, there was perovskite-like La_2NiO_4 in the fresh Ni–La_2O_3/5A catalyst. It is reasonable to speculate that during H_2-reduction, the aggregation of nickel atoms would be hindered by La_2O_3. Consequently, smaller nickel particles would be obtained in Ni–La_2O_3/5A. According to XRD estimation, the size (9 nm) of the nickel particles generated in Ni–La_2O_3/5A is much smaller than that (33 nm) observed over the Ni/La_2O_3 catalyst reported by Zhang *et al.* (23). Compared to the estimation of XRD results, the larger nickel particles deduced from CO chemisorption might be due to the suppression of CO chemisorption (37), a result of the isolation effect of La_2O_3 on nickel particles in the Ni-La_2O_3/5A catalyst. In other words, using La_2NiO_4 as a nickel precursor is a better means for producing fine Ni^0 particles. Supports which are basic have been reported to be capable of activating CO_2 and are favorable for the elimination of deposited carbons (5, 26). It has been pointed out that the Ni–La_2O_3/5A catalyst showed an affinity to CO_2 similar to that of 5A zeolite (38). From Table 2, one can observe that at 450°C, the TOFs of CH_4 and CO_2 are 0.21 and 0.28 s^{-1}, respectively, over Ni–La_2O_3/5A. Under similar experimental conditions, the corresponding TOFs are 0.01 and 0.01 s^{-1}, respectively, over 1 wt% Ir/Al_2O_3 (5, 11). These results suggested that Ni-La_2O_3/5A is an active catalyst for CO_2/CH_4 reforming. Generally speaking, there are two reasons for the deactivation of nickel-based catalysts in CO_2/CH_4 reforming: (i) the blocking of active sites by carbonaceous deposits (7, 23, 39, 40); and (ii) the sintering of nickel particles (1, 14, 41). We observed that the catalytic activity of Ni–La_2O_3/5A decreased gradually during 48 h of on-stream reaction. Since the size of nickel particles remained unchanged, one can affirm that Ni^0 sintering in Ni–La_2O_3/5A was not significant. Therefore, we suggest that the gradual degradation of the catalyst is mainly due to carbon deposition.

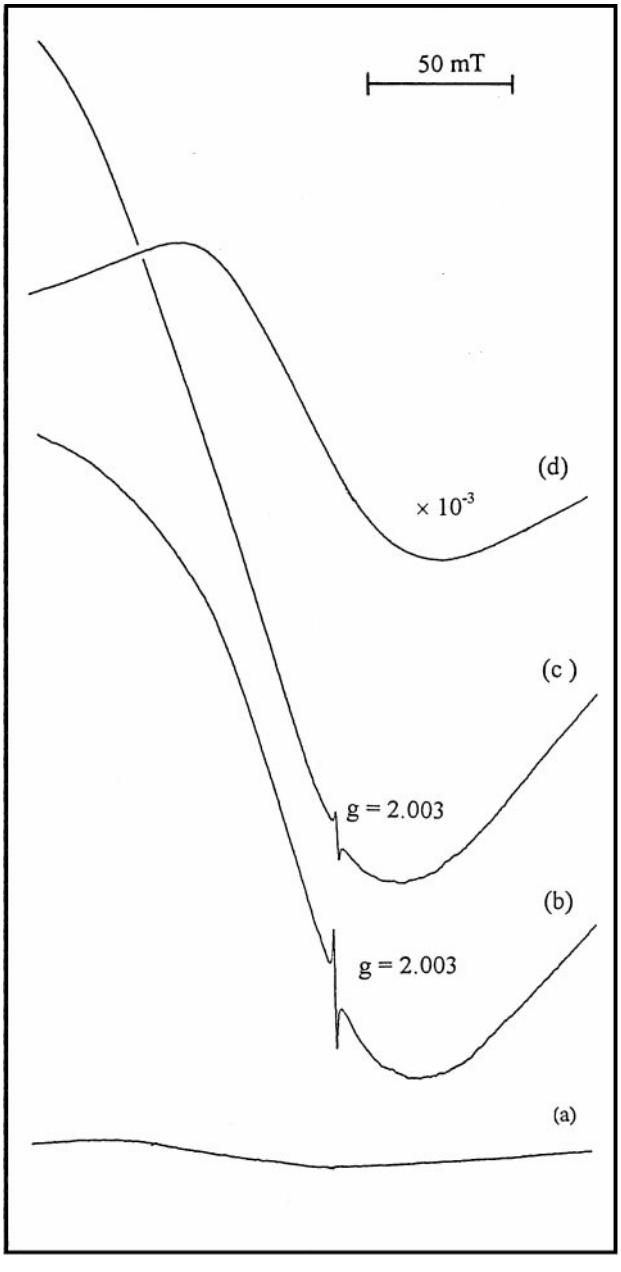

FIG. 12. EPR profiles of (a) fresh 0.5 wt% Ni–La_2O_3/5A; (b) 0.5 wt% Ni–La_2O_3/5A after H_2-reduced at 400°C; and (c) after purging with CO_2 for 30 min at 400°C; (d)10 wt% Ni–La_2O_3/5A after H_2-reduced at 500°C.

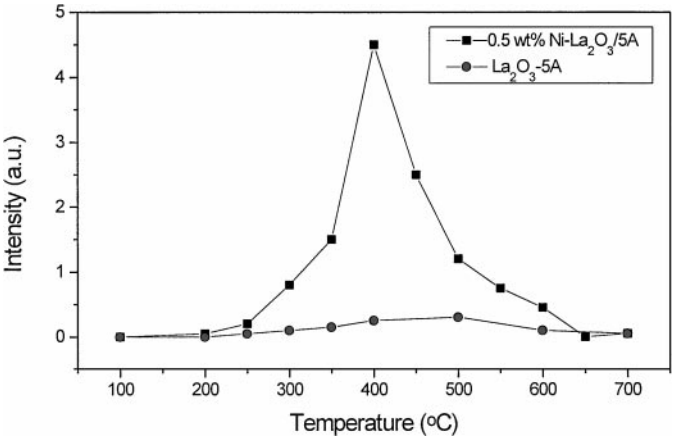

FIG. 13. The intensity of trapped electron signal as a function of H_2-reduced temperature over (●) La_2O_3/5A and (■) 0.5 wt% Ni–La_2O_3/5A.

2. *Carbon Deposition*

It has been pointed out that carbon deposition in CO_2/CH_4 reforming can deactivate nickel catalysts (21, 42). The deposition of carbon is mainly due to methane decomposition or CO disproportionation (5, 20, 37, 42, 43). Over Ni–La_2O_3/5A at 600 or 650°C, the conversion of CO_2 was higher than that of CH_4 (Table 2, Fig. 9). We attribute

that to the occurrence of the RWGS reaction as suggested before by other researchers (23, 25, 28, 44). At or above 700°C, it was the CH_4 conversion that was higher (Table 2 and Fig. 9). Both CH_4 decomposition and CO_2 complete dissociation (i.e., $CO_2 \rightarrow CO + O$ and then $CO \rightarrow C + O$; the surface oxygen adspecies can enhance CH_4 conversion (24–26)), would contribute to this phenomenon. As illustrated in Fig. 1, CO disproportionation can occur over the Ni–La_2O_3/5A catalyst. In other words, the CO originated in CO_2 decomposition can dissociate further to surface C and O.

The CO disproportionation process is exothermic and the equilibrium constant decreases with the rise in reaction temperature, whereas the decomposition of CH_4 is endothermic and the equilibrium constant increases with temperature rise. Reitmeier *et al.* (10) reported that for any reaction with a mixture of H_2, CO, CH_4, CO_2, and H_2O at thermodynamic equilibrium, the extent of graphitic carbon deposition decreased with temperature rise and the main cause for carbon deposition was CO disproportionation. With the increase in reaction temperature, we observed that the amount of deposited carbon decreased both in $CO_2/CH_4/N_2$ and CO/N_2 atmospheres but increased in an atmosphere of CH_4/N_2 (Fig. 3). According to the microscopic images (Fig. 2), there were the formations of filamentous whisker carbon in CO/N_2 and CO_2/CH_4 atmospheres and encapsulated carbon in CH_4/N_2. Since the morphology of the carbon deposited in CO_2/CH_4 is similar to that deposited in CO, we purpose that CO disproportionation is one of the main steps for carbon generation in CO_2 decomposition.

The observation of $^{13}CO_2$ and CO_2 in the pulsing of O_2 onto a H_2-reduced Ni–La_2O_3/5A sample formerly exposed to $^{13}CH_4/CO_2$ indicates that both CH_4 and CO_2 contribute to the accumulation of deposited carbon (Fig. 4). The $^{13}CO_2/CO_2$ molar ratio decreased with O_2 pulse number (Fig. 5), indicating that the ^{13}C species derived from $^{13}CH_4$ were more reactive toward O_2 than the ^{12}C species derived from CO_2. Compared to the carbon deposited in CO and CO_2/CH_4 exposures, the carbon deposited in CH_4 exposure could be removed more readily by CO_2 (Fig. 1); this is an indication that the carbon species generated in CH_4 dissociation are more reactive than those originated from CO or CO_2. With the increase in temperature, the $^{13}CO_2/CO_2$ molar ratio decreased (Fig. 6); i.e., the contribution of CO_2 toward carbon deposition via CO (formed in CO_2 dissociation) disproportionation increased with the rise in temperature. It is clear that carbon deposition is predominantly due to CO_2 dissociation and CO disproportionation at temperatures above 700°C.

3. Reaction Mechanism

3.1. The activation of CH_4 and CO_2. The mechanism of CO_2/CH_4 reforming has been extensively investigated. Shustorovich and Bell (45) argued that O-assisted CH_4 dissociation is energetically unfavorable on Ni surfaces. In a XPS study, Alstrup *et al.* (46) reported that the presence of oxygen adatoms on nickel did not enhance CH_4 activation. However, based on DRIFT and activity results, Solymosi *et al.* (29, 30) claimed that the adsorbed O_s generated in CO_2 dissociation facilitated the decomposition of CH_4. By means of vibrational spectroscopy, Quinlan *et al.* (47) investigated the interaction of methane with preadsorbed oxygen on a Ni(100) surface, they concluded that oxygen adatoms could promote the dissociative adsorption of methane. To evaluate the possibility of oxygen-assisted dissociation of methane, Au *et al.* (48) performed theoretical calculations to estimate the activation energies of hydrogen abstraction from methane in elementary steps with or without the involvement of adsorbed oxygen on a Ni (111) surface; they concluded that oxygen located at on-top site assists methane dissociation, as suggested previously by Hu and Ruckenstein (49).

The amount of CH_4 converted in 5 pulses of CH_4 at 600°C over a H_2-reduced Ni–La_2O_3/5A catalyst was 1.3 μl, and we observed no generation of C_2H_6, C_2H_4, CO_x, etc. in the outlet (Table 3). It indicated that the carbon species (such as deposited carbon, CH_x species) generated in CH_4 dissociation remained completely on the catalyst. When 337.5 μl of CH_4 was pulsed onto a H_2-reduced Ni–La_2O_3/5A catalyst pretreated with 5 pulses of CO_2 at 600°C (Table 2), CO was detected, indicating that there was interaction between CH_4 and the oxygen released in the dissociation of CO_2. Taking into consideration that the amount of converted CH_4 (8.8 μl) over the CO_2-treated catalyst was much more than that (1.3 μl) over the reduced catalyst, we propose that surface oxygen indeed promotes CH_4 decomposition. Similar observations were made at 700 and 800°C. Therefore, we advocate the idea of oxygen-assisted CH_4 dissociation. Of course, we do not exclude the possibility of direct methane dissociation on metallic nickel.

In contrast, the idea of H-assisted CO_2 activation has been generally accepted (5, 29, 30, 38). The observation of CD_3COOH in the CD_3I chemical trapping experiments suggests that HCOO is an intermediate in CO_2/CH_4 reforming. In the IR studies of CO_2/CH_4 reforming, bands attributable to surface formate were not detected over Ni/La_2O_3 (23, 37), Ni/SiO_2 (37), and Pt/TiO_2 (31), while over Ni/Al_2O_3 (37) and Rh/TiO_2 (5), they were detected. It is apparent that the presence of formate is closely related to the nature of the catalyst. The La_2O_3/5A support in the Ni–La_2O_3/5A catalyst exhibited large specific surface area (157 $m^2\ g^{-1}$) and good affinity to CO_2. These are favorable factors for the production of surface formate species. The existence of HCOO on the working catalyst indicates that adsorbed CO_2 could react with adsorbed H on nickel. According to the EPR results (Figs. 12 and 13), compared to La_2O_3/5A, more trapped electrons were generated in

0.5 wt% Ni–La_2O_3/5A during H_2 reduction. It is possible that Ni^0 promotes H_2 dissociation and the spillover of hydrogen from Ni^0 enhances the reduction of La_2O_3. The decrease in the intensity of trapped electron signal after the introduction of CO_2 suggested that CO_2 could pick up a trapped electron to form CO_2^-. Solymosi *et al.* (50) detected the IR signal of CO_2^- at 1325 and 1695 cm^{-1} on a K-modified Rh/SiO_2 catalyst. We envision that this CO_2^- species can react with surface H to produce formate species. As indicated by the activity data of Table 2 and Fig. 9, CO_2 conversion was higher than CH_4 conversion in CO_2/CH_4 reforming, possibly due to the RWGS reaction (5, 23, 25). This result is also a supporting evidence for the viewpoint that CO_2 dissociation can be activated by the surface hydrogen generated in CH_4 dissociation.

From Table 3, it can be seen that the total amount of CO (7.4 μl) produced in the first 5 pulses of CO_2 and in the following 5 pulses of CH_4 was much smaller than that (280 μl) generated in 10 pulses of CO_2/CH_4 at 600°C. Similar observations were made at 700 and 800°C. Therefore, we suggest that CH_4 and CO_2 can activate each other mutually.

3.2. Reaction intermediates. As for CH_4 activation, CH_4/CD_4 isotope effect has been investigated before (25, 51). A simplified expression of CH_4/CD_4 isotope effect for CO_2/CH_4 reforming is

$$k_H/k_D = \exp\left(-\left(E^0_{(H)} - E^0_{(D)}\right)/RT\right),$$

where k_H and k_D are the rate constants for CH_4/CO_2 and CD_4/CO_2 reactions and $E^0_{(H)}$ and $E^0_{(D)}$ the activation energies for spontaneous decomposition of hydrogen-containing and deuterium-containing adsorbed species, respectively. In the present study, we observed that with the increase in reaction temperature from 600 to 800°C, the deuterium isotope effect decreased (Fig. 9). This result is in accord with the equation for CH_4/CD_4 isotope effect. Zhang *et al.* (27) and Burghgraef *et al.* (52), respectively, reported experimental and theoretical results of similar nature. At 800°C, the CH_4 and CO_2 conversions over Ni–La_2O_3/5A were, respectively, 92.1 and 79.7%, suggesting that the reaction was close to the thermodynamic equilibrium. In other words, the reaction was controlled by thermodynamics rather than by kinetics (5). Therefore, no CH_4/CD_4 isotope effect was observed at 800°C. At 600°C, CH_4/CD_4 isotope effect for CH_4 conversion was 1.2 over Ni–La_2O_3/5A (Fig. 9). This result indicates that C–H cleavages are slow kinetic steps. There are three possible ways for C–H cleavages in CO_2/CH_4 reforming:

(i) $CH_4 \rightarrow C + 4H$

(ii) $CH_x + O \rightarrow CO + xH$

(iii) $CH_xO \rightarrow CO + xH$.

Among them, step (i) was believed to be reversible. In Fig. 10, one can observe that CH_4 and CD_4 conversions are nearly equal. Consequently, no kinetic isotopic effect was observed, indicating direct CH_4 dissociation is largely reversible over the reduced Ni–La_2O_3/5A. This is in concord with the conclusions drawn by Au *et al.* (48) and Hu *et al.* (49) based on theoretical calculations. After investigating isotopic scrambling between CH_4 and CD_4 during CO_2 reforming of CH_4 over Ni/SiO_2, Kroll *et al.* (53) pointed out that the decomposition of CH_4 was reversible. A similar conclusion was also reported by Bradford and Vannice (5, 21). By means of pulse surface reaction rate analysis (PSRA), Osaki *et al.* examined the CH_x intermediates during CO_2/CH_4 reforming over Co/Al_2O_3 (32) and Ni/Al_2O_3 (33), they proposed that step (ii) was rate-determining. According to the calculations on the surface reaction between CH_x and O, they concluded later that step (iii) was the rate-determining step (54). Considering zero activation energies for radical reactions between CH_x and OH as well as between CH_x and O in the gas phase (55), Bradford and Vannice (5, 21, 31) proposed that the dissociation of CH_xO to CO and H was rate-determining. Osaki *et al.* (32, 33, 54) and Bradford *et al.* (5, 21, 31), however, did not provide experimental evidences for such a suggestion. Our results of TG and CH_4–CO_2 pulsing experiments demonstrate that the deposited carbon deriving from CH_4 reacts with CO_2 rather readily (Figs. 1 and 5). The absence of CH_x adspecies over Ni/La_2O_3 (37) Ni/Al_2O_3 (37), Ni/SiO_2 (53) under reforming conditions had been confirmed by IR spectroscopic studies. These results indicated that the interaction of CH_x with surface oxygen species was fast. Thus we deduce that step (ii) is a combination of two elemental steps:

$$CH_x + O \rightarrow CH_xO$$

$$CH_xO \rightarrow CO + xH.$$

Since the former step is rather facile, we propose that the latter, i.e., step (iii), is rate-determining. The observation of CD_3CHO, D_2CO, and HDCO in CD_3I chemical trapping indicated that there was HCO species on the working catalyst. No CD_3OCH_3 was detected in CD_3I trapping and there was no CH_3OH detected in CO_2/CH_4 reforming; we suggest that there is no methoxy present on the surface during the reforming reaction. It has been reported that formate dissociates rather readily to formyl and formaldehyde in H_2 at high temperatures (56). Also, IR studies on formaldehyde adsorption demonstrated that H_2CO adsorption would give rise to formyl (56). Based on these understandings, we suggest that there were H_xCO ($x = 1$ or 2) species on the working Ni–La_2O_3/5A catalyst and the decomposition of H_xCO ($x = 1$ or 2) is rate-determining.

3.3. Reaction steps. Accordingly, we propose the following reaction pathways for CO_2/CH_4 reforming. There is mutual activation between CH_4 and CO_2. The

decomposition of CH_4 on Ni^0 can be assisted by the oxygen generated in CO_2 dissociation via CH_xO ($x = 1$ or 2) formation. The CO_2 adsorbed on the basic sites dissociates with or without the aid of surface H species. The rate-determining step is the dissociation of CH_xO ($x = 1$ or 2) to CO and H. The chemical equations involved are

$$CH_{4,s} \rightarrow CH_{x,s} + (4 - x)H_{,s} \quad [1]$$

$$CO_{2,s} \rightarrow CO_{,s} + O_{,s} \quad [2]$$

$$CH_{4,s} + O_{,s} \rightarrow CH_xO_{,s} + (4 - x)H_{,s} \quad [3]$$

$$CO_{2,s} + xH_{,s} \rightarrow CH_xO_{,s} + O_{,s} \quad [4]$$

$$CH_xO_{,s} \rightarrow CO + xH_{,s} \qquad (s = \text{surface}). \quad [5]$$

CONCLUSIONS

Ni–La_2O_3/5A exhibited good catalytic performance for CO_2/CH_4 reforming. Such activity could be related to the small metallic nickel crystallites (ca. 9 nm) generated on/in perovskite-like La_2NiO_4. Carbon deposition is the main reason for catalytic deactivation. The deposited carbon could be originated from both CH_4 and CO_2; at higher temperatures, the contribution of CO_2 was more significant. Based on the facts that the TG profiles and TEM imagines of carbon formed in CO and CO_2/CH_4 atmospheres are very similar, we suggest that carbon deposition was mainly via CO disproportionation. The existence of H (or O) species on the catalyst surface could promote the activation of CO_2 (or CH_4) significantly; a result of CO_2 and CH_4 mutual activation. We have proposed reaction pathways for the reforming reaction and suggested that CH_xO ($x = 1$ or 2) decomposition is a rate-determining step.

ACKNOWLEDGMENTS

The work described above was fully supported by a grant from the Research Grants Council of the Hong Kong Special Administration Region, China (Project No. HKBU 2053/98 P). We thank Prof. B. L. Zhang of Chengdu Institute of Organic Chemistry, Chinese Academy of Sciences for performing the TEM investigation.

REFERENCES

1. Chubb, T. A., *Sol. Energy* **24**, 341 (1980).
2. Mccrary, J. H., Mccrary, G. E., Chubb, T. A., Nemecek, J. J., and Simmons, D. E., *Sol. Energy* **24**, 141 (1982).
3. Fish, J. D., and Haun, D. C., *J. Sol. Energy Eng.* **109**, 215 (1987).
4. Edwards, J. H., Do, K. T., Maitra, A. H., Schuck, S., and Stein, W., *Sol. Eng.* **1**, 389 (1995).
5. Bradford, M. C. J., and Vannice, M. A., *Catal. Rev.—Sci. Eng.* **41**(1), 1 (1999).
6. Nishiyama, T., and Aika, K. I., *J. Catal.* **122**, 346 (1990).
7. Sodesawa, T., Dobashi, A., and Nozaki, F., *React. Kinet. Catal. Lett.* **12**, 107 (1979).
8. Gadalla, A. M., and Bower, B., *Chem. Eng. Sci.* **43**, 3049 (1988).
9. Sacco, A., Jr., Geurts, F. W. A. H., Jablonski, G. A., Lee, S., and Gately, R. A., *J. Catal.* **119**, 322 (1989).
10. Reitmeier, R. E., Atwood, K., Bennet, H. A., Jr., and Baugh, H. M., *Ind. Eng. Chem.* **40**, 620 (1948).
11. Perera, J. S. H. Q., Couves, J. W., Sankar, G., and Vernon, P. D. F., *Nature* (London) **35**, 225 (1991).
12. Ashcroft, A. T., Cheetham, A. K., Green, M. L. H., and Thomas, J. M., *Catal. Lett.* **11**, 219 (1991).
13. Yamazaki, O., Nozaki, T., Omata, K., and Fujimoto, K., *Chem. Lett.* 1953 (1992).
14. Zhang, Z. L., and Verykios, X. E., *Catal. Today* **21**, 589 (1994).
15. Horiuchi, T., Sakuma, K., Fukui, T., Kubo, Y., Osaki, T., and Mori, T., *Appl. Catal. A: General* **144**, 111 (1996).
16. Chen, Y. G., and Ren, J., *Catal. Lett.* **29**, 39 (1994).
17. Sridhar, S., Du, S., and Seetharaman, S., *Z. Metallkd.* **85**, 616 (1994).
18. Bhattacharyya, A., and Chang, V. W., *Stud. Surf. Sci. Catal.* **88**, 207 (1994).
19. Hu, Y. H., and Ruckenstein, E., *Catal. Lett.* **36**, 145 (1996).
20. Tomishige, K., Chen, Y. G., and Fujimoto, K., *J. Catal.* **181**, 91 (1999).
21. Bradford, M. C. J., and Vannice, M. A., *Appl. Catal. A: General* **142**, 73 (1996); **142**, 97 (1996).
22. Zhang, Z. L., and Verykios, X. E., *J. Chem. Soc., Chem. Commun.* 71 (1995).
23. Zhang, Z. L., Verykios, X. E., MacDonald, S. M., and Affrossman, S., *J. Phys. Chem.* **100**, 744 (1996).
24. Wang, H. Y., and Au, C. T., *Catal. Lett.* **38**, 77 (1996).
25. Wang, H. Y., and Au, C. T., *Appl. Catal. A: General* **155**, 239 (1997).
26. Kim, G. J., Cho, D. S., Kim, K. H., and Kim, J. H., *Catal. Lett.* **28**, 41 (1994).
27. Zhang, Z. L., and Verykios, X. E., *Catal. Lett.* **38**, 175 (1996).
28. Nakamura, J., Aikawa, K., Sato, K., and Uchijima, T., *Catal. Lett.* **25**, 265 (1994).
29. Solymosi, F., Kustan, Gy., and Erdöhelyi, A., *Catal. Lett.* **11**, 149 (1991).
30. Erdöhelyi, A., Fodor, K., and Solymosi, F., *Stud. Surf. Sci. Catal.* **107**, 525 (1997).
31. Bradford, M. C. J., and Vannice, M. A., *J. Catal.* **173**, 157 (1998).
32. Osaki, T., Masuda, H., and Mori, T., *Catal. Lett.* **29**, 33 (1994).
33. Osaki, T., Masuda, H., Horiuchi, T., and Mori, T., *Catal. Lett.* **34**, 59 (1995).
34. Melander, L., "Isotopic Effects on Reaction Rates." Ronald Press, New York, 1960.
35. Deluzarche, A., Hindermann, J. P., Kiennemann, A., and Kieffer, K., *J. Mol. Catal.* **31**, 225 (1985).
36. Qiu, Z. W., "Electron Spin Resonance Spectroscopy." Academic Press, San Diego, 1980.
37. Tsipouriari, V. A., Zhang, Z. L., and Verykios, X. E., *J. Catal.* **179**, 283 (1998); Tsipouriari, V. A., Verykios, X. E., *J. Catal.* **187**, 85 (1999).
38. Luo, J. Z., Gao, L. Z., Yu, Z. L., and Au, C. T., *Stud. Surf. Sci. Catal.* **130**, 689 (2000).
39. Bitter, J. H., Seshan, K., and Lercher, J. A., *J. Catal.* **183**, 336 (1999).
40. Rostrup-Nielsen, J. R., and Bak Hansen, J. H., *J. Catal.* **144**, 38 (1993).
41. Tsipouriari, V. A., Efstathiou, A. M., Zhang, Z. L., and Verykios, X. E., *Catal. Today* **21**, 579 (1994).
42. Zhang, Z. L., and Verykios, X. E., *Appl. Catal. A: General* **138**, 109 (1996).
43. Swaan, H. M., Kroll, V. C. H., Martin, G. A., and Mirodatos, C., *Catal. Today* **21**, 571 (1994).
44. Erdöhelyi, A., Cserenyi, J., and Solymosi, F., *J. Catal.* **141**, 287 (1993).
45. Shustorovich, E., and Bell, A. T., *Surf. Sci.* **248**, 397 (1992).

46. Alstrup, I., Chorkendorff, I., and Ullmann, S., *Surf. Sci.* **234**, 79 (1990).
47. Quinlan, M. A., Wood, B. J., and Wise, H., *Chem. Phys. Lett.* **118**(5), 478 (1985).
48. Au, C. T., Liao, M. S., and Ng, C. F., *J. Phys. Chem. A* **102**, 3959 (1998).
49. Hu, Y. H., and Ruckenstein, E., *Catal. Lett.* **34**, 41 (1995).
50. Solymosi, F., and Knözinger, H., *J. Catal.* **122**, 166 (1990).
51. Osaki, T., Horiuchi, T., Suzuki, K., and Mori, T., *J. Chem. Soc. Faraday Trans.* **92**, 1627 (1996).
52. Burghgraef, H., Jansen, A. P. J., and van Santen, R. A., *J. Chem. Phys.* **101**, 11,012 (1994).
53. Kroll, V. C. H., and Swaan, H. M., and Mirodatos, C., *J. Catal.* **161**, 409 (1996).
54. Osaki, T., Fukaya, H., Horiuchi, T., Suzuki, K., and Mori, T., *J. Catal.* **180**, 106 (1998).
55. Miller, J. A., and Bowman, C. T., *Prog. Energy Comb. Sci.* **15**, 287 (1989).
56. Edwards, J. F., and Schrader, G. L., *J. Phys. Chem.* **89**, 782 (1985).